JOURNAL OF AIRCRAFT
Vol. 42, No. 6, November–December 2005

Detached Eddy Simulations for Iced Airfoils

Jianping Pan* and Eric Loth†
University of Illinois at Urbana–Champaign, Urbana, Illinois 61801-2953

To improve the predictive ability of the stall behavior for iced airfoils, computations using the detached eddy simulation (DES) approach were conducted. The WIND code with the DES methodology was first validated with a well-documented flow past a circular cylinder. The validation results were in good agreement with the experimental and previous numerical results for the time-averaged aerodynamic forces, as well as for the unsteady flowfield pattern. DES computations were then performed for a series of angles of attack (around the stall angle) for NACA 23012 and natural laminar flow (NLF) 0414 airfoils with a simulated (two-dimensional) ice shape on the upper surface. The spanwise domain for these simulations was scaled based on the expected height of the separation region, consistent with previous blunt-body large eddy simulation and DES. The DES for both iced airfoils provided the maximum lift coefficients and stall angles that were qualitatively consistent with experiments [whereas Reynolds-averaged Navier–Stokes (RANS) simulations of the same cases failed to provide either such behavior]. However, the DES approach was much more computationally intensive, and even higher grid resolution within the separated flow region is suggested to improve the predictive performance for this technique.

Introduction

AIRCRAFT aerodynamic degradation due to significant ice accretion is a severe problem faced by pilots and has caused many accidents. Ice accretion alters the airfoil geometry, and its induced early flow separation can severely reduce the lift, increase the drag, change the pitch and hinge moments, and lead to loss in control effectiveness. Although aircraft icing and its resulting hazards have been noticed and studied for a quite long period, it is still a contributing or casual factor in approximately 10% of all weather-related accidents among general aviation aircraft in recent years.[1] Further understanding of the ice accretion's aerodynamic effects is important to help assess the aircraft's potential capability during ice conditions.

Numerical simulation has become common in the last two decades and is now playing an important role because it is often a less expensive alternate investigation tool. With the dramatic progress of computer speed and memory in recent years, numerical simulations of iced airfoils have made significant improvements in predictive performance. Most of the studies have been based on Reynolds-averaged Navier–Stokes (RANS) methodology due to its moderate computer resource requirement. In the RANS method, the viscous turbulent effects are resolved using time-averaged closure models. The RANS methodology has allowed much in the prediction of mean flow properties and the integrated aerodynamic forces for clean and iced airfoils. It is a common technique because it allows efficient predictions for a wide variety of flows and configurations.[2]

However, RANS cannot robustly capture the nonlinear detachment process associated with ice-shape vortex shedding and, thus, has difficulty in predicting iced airfoil aerodynamics, especially near stall conditions.[2–4] In particular, it is often unable to reproduce experimentally determined stall angles and stall behavior. This lack of accurate prediction has motivated examination of other approaches. Two available methodologies that can capture aspects of the unsteady vortex structures that govern stall separation are direct numerical simulation (DNS) and large eddy simulation (LES). In DNS, flow patterns for all of the turbulence scales (down to the Kolmogorov scales) are directly solved through the full unsteady Navier–Stokes equations. However, due to the limitation of current computational power, DNS has only been applied in low Reynolds number flows with simple boundary conditions. In airfoil flows, the typical Reynolds number is often more than 10^6, which is far beyond the capability of DNS. LES is a methodology that is in between RANS and DNS in terms of resolving the turbulence field and the required computational resources. In LES, vortices larger than the grid size are directly solved by the filtered Navier–Stokes equations, whereas only the subgrid-scale turbulent structures are empirically modeled. As a result, LES can be applied in separated (free-shear) flow regions for a reasonable range of Reynolds numbers. However, for high Reynolds number wall-bounded flows without separation, the dominant eddy structures near the wall are extremely small. Therefore, the grid resolution required for the attached boundary layers is intensive, such that LES is impractical for airfoils because at least some of the boundary layer is attached even in stalled conditions. As such, hybrid methodologies that combine LES and RANS approaches have been developed especially for these kinds of flows.

Detached eddy simulation (DES) is a recently developed hybrid LES–RANS methodology with the aim of robustly predicting high Reynolds number massively separated wall-bounded flows.[5] In the DES methodology, LES is implicitly combined with RANS by altering the length scale in the conventional RANS turbulence model. Unlike the zonal method where the RANS and LES regions are explicitly specified by the user, DES simply modifies the wall-normal length scale d in the wall destruction term to $\tilde{d} = \min(d, C_{\mathrm{DES}}\Delta)$, such that the method adapts to the wall distance and the grid resolution. In this definition, Δ is the maximum local grid spacing, that is, $\Delta = \max(\Delta x, \Delta y, \Delta z)$, and C_{DES} in an empirical constant of order unity. Thus, the DES technique is a nonzonal approach for treating the unsteady three-dimensional separated flows at high Reynolds numbers. In the boundary-layer region where Δ far exceeds d, the Spalart–Allmaras (S–A) model rules because $\tilde{d} = d$. In the massive flow separation region, where $\tilde{d} = C_{\mathrm{DES}}\Delta$, the DES turbulence model turns into a simple one-equation subgrid-scale (SGS) model, thus yielding an LES approach. If the momentum-carrying turbulent eddies are not much smaller than the scale of the geometry, then the separated flow might be well resolved with only moderate grid refinement.

In recent years, DES has been successfully applied to a range of massively separated flows and has provided promising predictions. This has included the studies on clean airfoils at various angles of attack[6] and cylinders, sphere, and forebody flows under sub- and supercritical Reynolds number conditions.[7–9] Whereas the limited

Presented as Paper 2004-0564 at the AIAA 42nd Aerospace Sciences Meeting, Reno, NV, January 2004; received 29 June 2004; revision received 25 August 2004; accepted for publication 5 October 2004.

*Graduate Research Assistant, Department of Aerospace Engineering. Student Member AIAA.

†Professor, Department of Aerospace Engineering, 306 Talbot Laboratory, 104 South Wright Street; loth@uiuc.edu. Member AIAA.

DES studies to date are for rather simple configurations, Kumar and Loth[10] presented some preliminary DES results for an iced natural laminar flow (NLF) 0414 airfoil with a $k/c = 6.67\%$ ice shape at a leading-edge location. The results indicated that three-dimensional flow structures were well represented when different spanwise planes were examined. However, in this preliminary study only two angles of attack were considered with a low-resolution grid and the mean aerodynamic forces were not examined for a statistically long period. As such, the authors suggested that a detailed set of simulations be conducted with comparison to experimental data to investigate the potential improvements in the prediction accuracy of DES (as compared to RANS) for iced airfoil simulations with significant flow separations. In this study, such DES simulations were performed for iced NACA 23012 and NLF 0414 airfoils with typical leading-edge and upper-surface ice shapes. The results were compared to the low-turbulence pressure tunnel (LTPT) and University of Illinois Urbana–Champaign (UIUC) experimental data conducted by the UIUC Icing Group and also to the previous RANS simulation results.

Computational Methodology

A structured Navier–Stokes equation solver WIND[11] was primarily applied in this study. Although WIND 5.0 includes various one-equation and two-equation turbulence models for its RANS computations, its DES method is based on the S–A one-equation model. This DES method was chosen herein as the hybrid LES–RANS method also because the S–A model yielded good performance in comparison to other turbulence models for RANS predictions of iced airfoils (see Refs. 2–4).

In the conventional (S–A) model[12] turbulent viscosity μ_t is solved by a partial differential equation as follows, where d in the wall destruction terms is the distance to the closest wall:

$$\frac{\mathrm{D}\tilde{\nu}}{\mathrm{D}t} = C_{b1}[1 - f_{t2}]\tilde{S}\tilde{\nu} + \frac{1}{\sigma}\left[\nabla((\nu + \tilde{\nu})\nabla\tilde{\nu}) + C_{b2}(\nabla\tilde{\nu})^2\right] - \left[C_{w1}f_w - \frac{C_{b1}}{k^2}f_{t2}\right]\left[\frac{\tilde{\nu}}{d}\right]^2 + f_{t1}\Delta U^2$$

In the DES method, the length scale d is replaced by $\tilde{d} = C_{\mathrm{DES}}\Delta$. With this altered length scale, the S–A RANS approach will be applied in the region close to wall because the wall distance d is small and Δx or Δz in the stretched RANS grid is large in comparison such that $\tilde{d} = d$. However, the wall distance above the boundary layer is much larger than its local grid size, which yields $\tilde{d} = C_{\mathrm{DES}}\Delta$. As such, the conventional S–A model turns out to be a one-equation model for an SGS eddy viscosity:

$$\frac{\mathrm{D}\tilde{\nu}}{\mathrm{D}t} = C_{b1}[1 - f_{t2}]\tilde{S}\tilde{\nu} + \frac{1}{\sigma}\left[\nabla((\nu + \tilde{\nu})\nabla\tilde{\nu}) + C_{b2}(\nabla\tilde{\nu})^2\right] - \left[C_{w1}f_w - \frac{c_{b1}}{k^2}f_{t2}\right]\left[\frac{\tilde{\nu}}{C_{\mathrm{DES}}\Delta}\right]^2$$

The algebraic Smagorinsky subgrid stress model, in which $\tilde{\nu} = C_D\tilde{S}\Delta^2$, can be recovered from this equation if the production term and wall destruction terms are balanced out as

$$C_{b1}(1 - f_{t2})\tilde{S}\tilde{\nu} - \left[C_{w1}f_w - \left(C_{b1}/k^2\right)f_{t2}\right](\tilde{\nu}/C_{\mathrm{DES}}\Delta)^2 = 0$$

$$\tilde{\nu} = C_{\mathrm{DES}}^2 C_{b1}(1 - f_{t2})\tilde{S}\Delta^2 \Big/ \left[C_{w1}f_w - \left(C_{b1}/k^2\right)f_{t2}\right] \sim C_D\tilde{S}\Delta^2$$

As in the Smagorinsky SGS model, there is one grid-related parameter constant that needs to be set. The constant value of $C_{\mathrm{DES}} = 0.65$, set via validation with homogeneous turbulence by Shur et al.,[6] is used in this study. Other values were also examined, but the influence was generally not significant for values between 0.2 and 1. The DES method combines the strength of RANS in the wall-bounded region (modeling the average properties of attached flow turbulence) and LES in the free vortex shedding region (resolving eddies larger than the local grid size). Therefore, like LES, the DES methodology is unsteady and three dimensional because it seeks to describe (low-frequency) aspects of turbulent dynamics. However, in consideration of the computational cost for parametric studies, two-dimensional DES simulations were first conducted to investigate time-dependence and grid resolution aspects with a pseudospanwise grid spacing specified. In two-dimensional DES, a constant Δz, with the same value as in three-dimensional grid configurations, was specified when determining the LES/RANS interface. Although this restricts any streamwise vorticity (and, thus, is not physical in terms of emulating large-scale turbulence), it allowed similarity to a three-dimensional simulation for the resolution tests but with much less computational burden (though dependence on Δz and spanwise domain length would need to be determined via full three-dimensional simulations).

A single-block O-type structured grid was generated from the airfoil surface to 20 chords length away in all directions by using the grid generator software Gridgen. The nondimensional first grid spacing in the normal direction was set as 2×10^{-6}, consistent with a y^+ of about (or less than) one for the simulated flow conditions. In general, 400 points were distributed along the airfoil surface (with about 100 points along the ice shape), and 100 points were assigned in the normal direction. The grid distribution was clustered on the region where high flowfield gradients were expected, such as the leading-edge, trailing-edge, and ice-shape locations. Though simple, the use of a single block for the grid generation was attractive because it avoids complexities when dealing with ice-shape protuberances. For three-dimensional simulations, about 30 points were evenly distributed along the span.

The boundary conditions were specified through a grid preprocessor program included in WIND software package, GMAN. All cases included a viscous wall boundary condition on the airfoil surface and freestream boundary condition on the far-field boundary. For the three-dimensional DES simulations, a periodic boundary condition was specified along the spanwise direction. Because a three-dimensional calculation requires large computer resources, it is efficient to run such simulations in parallel with small divided zones. CFSPLIT, a WIND utility program, was, thus, used to split the whole grid into fractions. On the interface between different split zones, a zonal coupled boundary was specified. A more detailed DES methodology description applied in this study can be found in Ref. 13.

DES Results and Discussion

Validation for Cylinder

To examine its capability, the DES methodology (via the WIND code) was first validated with a well-documented cylinder flow. The applied numerical scheme for spatial discretization was a second-order upwind scheme. Higher-order schemes were desired, but were not used because they produced instabilities with WIND unless a very small (impractical) time step was used. For temporal discretization, a two-layer implicit MacCormack scheme was employed because it allowed a substantially larger time step compared to the explicit schemes, such that the total CPU time for a given physical time integration was significantly reduced. The current simulation results were compared with experimental data[14,15] and previously reported computational results.[7]

Computations were performed for the cylinder flow with several different Reynolds numbers, 5×10^4, 1.4×10^5, and 3.0×10^6 based on the freestream speed U_∞ and the cylinder diameter D. Herein, the 3.0×10^6 results are presented because this Reynolds number is most relevant to the iced airfoil flow because it yields turbulent boundary-layer separation under this condition. This was also computationally convenient because one could assume that transition occurs so quickly that the entire boundary layer from the stagnation point can be considered turbulent.

In the two-dimensional DES simulations, a viscous wall boundary condition was used on the cylinder and a freestream condition was used on the outer boundary at about 15 diameters away from cylinder. Grid-resolution and time-step dependence studies were first performed with two-dimensional DES simulations because fewer computer resources were required. These results were used to construct three-dimensional DES conditions where the spanwise

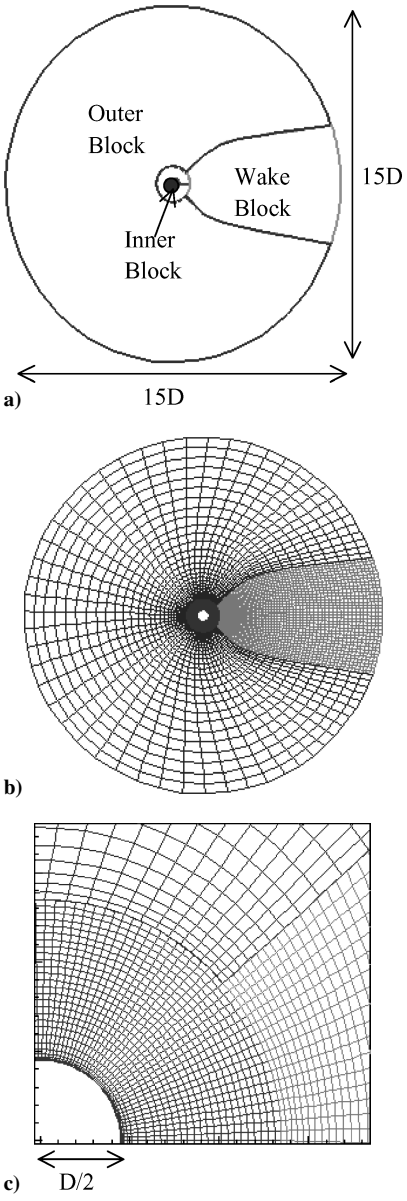

Fig. 1 Computational grid for cylinder flow simulations with inner block of 150 × 36, wake block of 74 × 36, and outer block of 59 × 30, with spanwise direction of 42: a) block schematic, b) overall grid, and c) grid near rear of cylinder.

grid resolution was the same as that used by Travin et al., which had 42 points over a spanwise length of two diameters.[7] In the three-dimensional DES simulation, the spanwise dimension employed periodic boundary conditions. Figure 1 shows the three-zone grid applied in the three-dimensional study. The inner block, wake block, and outer block have dimensions of $150 \times 30 \times 42$, $37 \times 74 \times 42$, and $75 \times 37 \times 42$, respectively. The inner block and wake block had finer grid resolutions because the main flow structure mostly formed within those regions. A grid aspect ratio of around unity was kept in the wake zone because the vortex structures are assumed to be relatively homogeneous in all three directions.

In the three-dimensional DES case, simulations were completed with a nondimensional time step ($\Delta t^* = \Delta t U_\infty / D$) of 0.01. This was found to provide time-independent statistical results in two-dimensional DES investigations (as shown in Table 1). Each computation cycle in the three-dimensional case took approximately 5 s per CPU with 27 clustered workstation processors running in parallel. The total integration time T^*_{int} was long enough to ensure statistically stationary time-averaged results.

Table 1 shows the predicted C_d and $C_{l,\text{rms}}$ with different grid resolutions and time steps for two-dimensional cases and a single three-dimensional case. The values were obtained by averaging the unsteady aerodynamic data after an initial transient period, typically from $t^* = 0$ to 20, where nondimensional time t^* was scaled by D/U_∞. When two-dimensional DES results based on the 300×208 grid and the 150×104 grid were compared, it was found that there was some grid-resolution influence and that improved resolution tends to give better predictions. Similarly, decreasing the time step from 0.01 to 0.005 gave an improvement as well, especially for the unsteady aspects. However, because the three-dimensional equivalent runs were intensive, the 150×104 grid with $\Delta t^* = 0.01$ was chosen for the three-dimensional DES case. Note that this is very similar to the resolution used by Travin et al. with the same time step.

Table 1 Summary of circular cylinder results, $M = 0.3$ and $Re = 3 \times 10^6$

Case	Grid	Δt^*	T^*_{int}	C_d	$C_{l,\text{rms}}$
Two-dimensional DES	300×208	0.0025	75	0.879	0.866
Two-dimensional DES	150×104	0.005	100	0.880	0.822
Two-dimensional DES	150×104	0.01	400	0.896	0.971
Three-dimensional DES	$150 \times 104 \times 42$	0.01	150	0.722	0.359
Two-dimensional URANS	150×104	0.01	200	0.864	0.969
Experiment	——	——	——	0.5–0.8	0.05–0.13

Figure 2 shows the instantaneous vorticity shedding structures. The three-dimensional vortex isosurface is shown in Fig. 2a, whereby one can clearly note the Kelvin–Helmholtz vortex shedding structures, as well as the streamwise vorticity features, denoted at low Reynolds number conditions as "vortex tubes" by Lasheras and Choi.[16] Figures 2b–2d show the vorticity contours at several different spanwise locations ($z/Z_{\text{dom}} = \frac{1}{6}$, $\frac{1}{2}$, and $\frac{5}{6}$), where significant three-dimensional variation can be found. Compared with the two-dimensional vorticity contours shown in Fig. 2e, a finer vortex structure was resolved in the three-dimensional results. This was attributed to the inclusion of streamwise vorticity interactions.

Figure 3 shows the histories of the lift and drag coefficient for two-dimensional and three-dimensional DES cases (150×104 and $150 \times 104 \times 42$). The predicted Strouhal number $Sr(fU_\infty/D)$ is about 0.25 for both cases, which was within the range from 0.2 to 0.28 given by the experimental data. Thus, the unsteady frequency was reasonably represented by both cases. However, the three-dimensional DES result was more stochastic (complex) and exhibited smaller amplitudes in the lift fluctuations. Both of these characteristics were more in line with experimental results for $C_{l,\text{rms}}$ as shown in Table 1, which is expected because the turbulent mixing, even at large scales, is sensitive to three dimensionality. As such, completion of two-dimensional DES is only recommended for investigating time-step and two-dimensional grid-dependency issues, but three-dimensional DES is needed for proper simulation.

Figure 4 shows the pressure distribution around the cylinder predicted by the three-dimensional DES and two-dimensional DES simulations. Compared to the experimental results, the C_p profile was well predicted by the three-dimensional DES, whereas the two-dimensional DES predicted a lower C_p, especially in the region where separation occurs. This indicates that, like the LES and DNS methods, DES requires a three-dimensional description of the vortices.

As shown in Table 1, the average drag coefficient of 0.72 predicted by three-dimensional DES fits reasonably in the range from 0.5 to 0.8 of the experimental results,[14,15] whereas a one-third higher drag was predicted by the two-dimensional DES. The similar prediction trend between the two- and three-dimensional DES cases was also found in the DES results by Travin et al.[7] Finally, note that two-dimensional unsteady Reynolds-averaged Navier–Stokes (URANS) is similar to two-dimensional DES for the same time step and grid resolution, indicating that the detailed nature of the subgrid stress model might not be critical for these flows in terms of predicting lift and drag forces.

The preceding results indicate that the WIND three-dimensional DES code reasonably predicted the main aerodynamic features

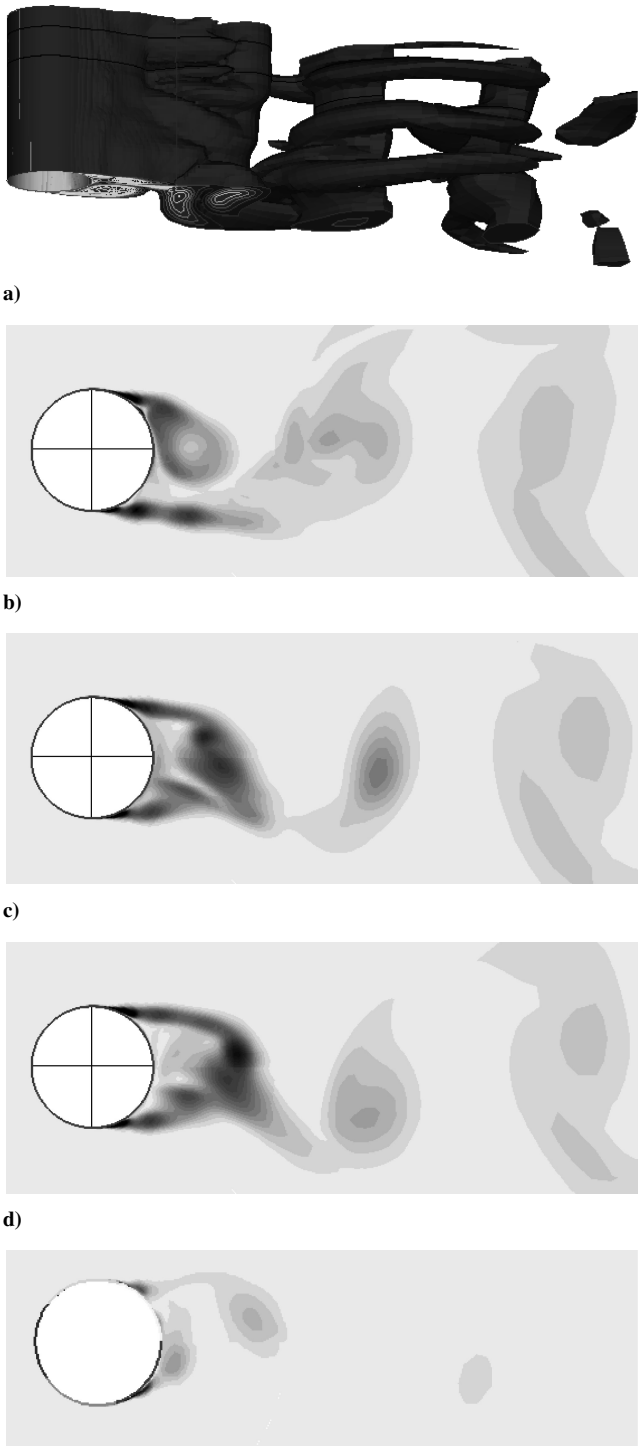

Fig. 2 Instantaneous vorticity contours for cylinder flow at $t^* = 120$: a) three-dimensional DES vorticity isosurface, b) three-dimensional DES at $z = \frac{1}{6}\ Z_{\text{dom}}$, c) three-dimensional DES at $z = \frac{1}{2}\ Z_{\text{dom}}$, d) three-dimensional DES at $z = \frac{5}{6}\ Z_{\text{dom}}$, and e) two-dimensional DES.

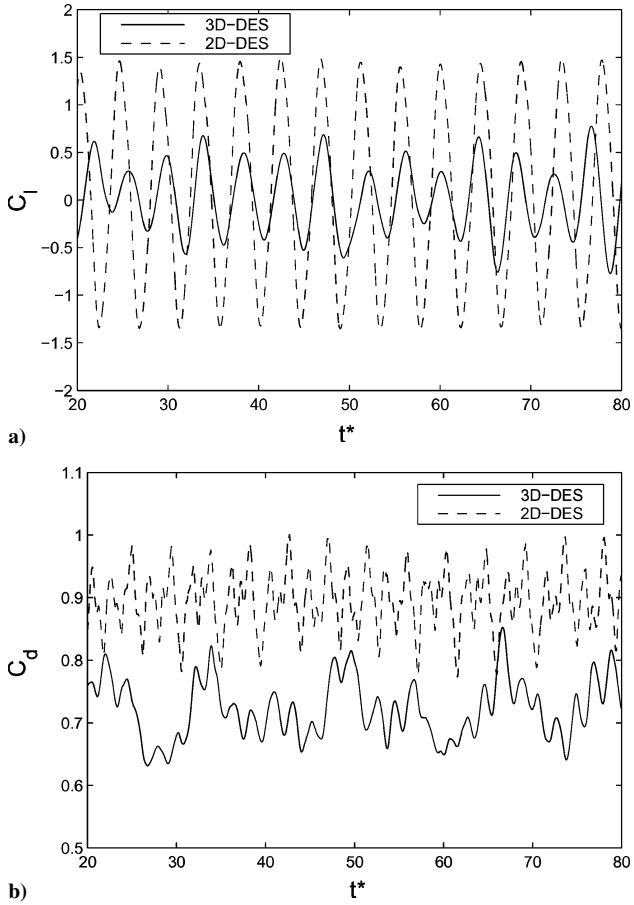

Fig. 3 History of a) lift coefficient and b) drag coefficient for circular cylinder flow.

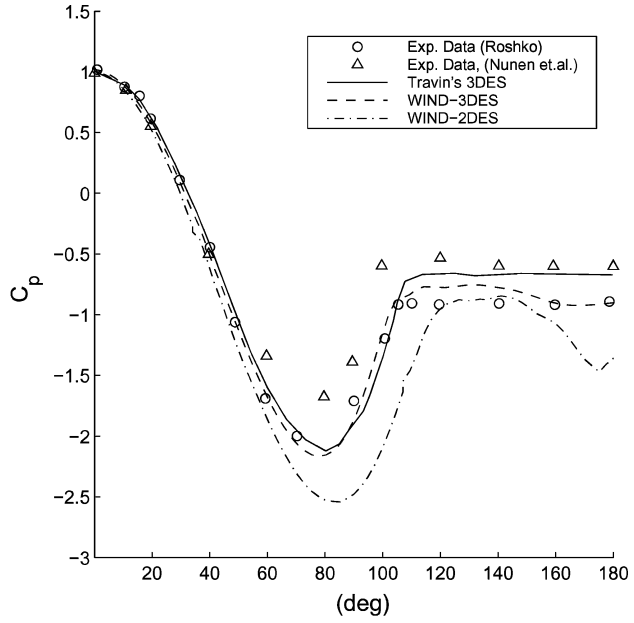

Fig. 4 Surface pressure distribution on circular cylinder with turbulent separation.

associated with a turbulent separated circular cylinder flow after careful comparison to experimental data and previous numerical predictions. This gave encouragement to apply DES in the iced airfoil simulations considering similarities between unsteady iced airfoil flow separation and the cylinder flow separation.

Assessment of Two-Dimensional DES on Airfoils

To assess DES performance for iced airfoil simulations, a series of numerical studies, including a grid resolution study, a time-step study, and a DES-region sensitivity study, were first investigated for a selected iced airfoil case. Because the full three-dimensional calculation required large computer resources, those aspects of the numerical studies were mainly performed with two-dimensional DES, as was done for the cylinder case. The chosen airfoil configuration was a quarter-round ice shape with $k/c = 1.39\%$ located on the NACA 23012 airfoil at 10% of chord length.

Simulations were performed at a Reynolds number of 2.1×10^6 and Mach number of 0.21. Those conditions were chosen because

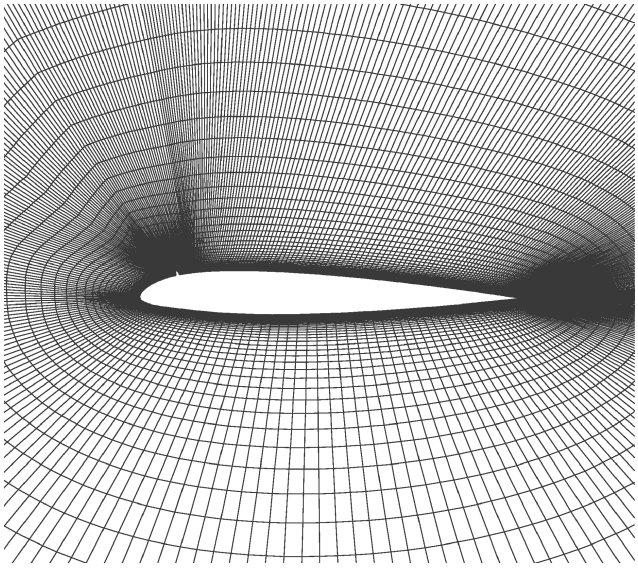

a)

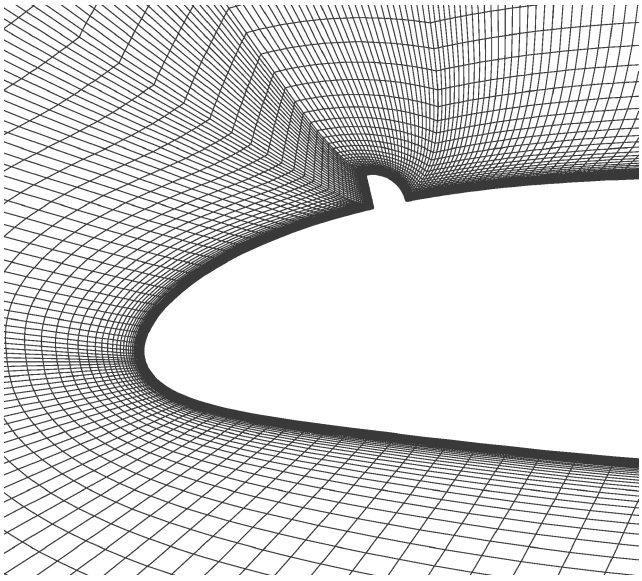

b)

Fig. 5 Computational grid for iced NACA 23012 airfoil: a) around airfoil and b) closeup near leading edge.

there are experimental results by Broeren et al.[17] available for comparison. In addition, these conditions were comparable to the cylinder validation case, and again the boundary layers were assumed to be turbulent everywhere for computational convenience.

A grid dimension of 400×100 was found reasonable in previous RANS studies for the iced airfoils.[2] To check if this grid resolution was also suitable for the DES methodology, grid-independence studies were performed for the selected iced airfoil case at a 7-deg angle of attack. A typical computational grid for the iced airfoil is shown in Fig. 5 (around the airfoil and close up near the leading edge). This grid was slightly adjusted from the grid used for the RANS simulations to keep a unit grid aspect ratio in the upper surface flow separation region.

Three different grid resolutions (500×125, 400×100, and 300×75) were selected for the two-dimensional DES calculation. Table 2 shows the averaged C_l and C_d results, as well as RANS values and available experimental data. Significant differences were found between the results based on the coarsest grid and on the other two finer grids, whereas between the two finer grid predictions, the difference was not significant, especially for the lift predictions. The significant discrepancy within the results indicates that DES methodology is much more grid sensitive than the RANS methodology, in which the differences would not be as great. This is because the DES methodology is sensitive not just to gradients in the flow (as is the RANS methodology) but to the resolution of specific vortex structures. Thus, the eddy cascade and turbulent mixing in the separated flow regions are a strong function of the grid.

Table 2 Grid study for iced NACA 23012 at $\alpha = 7$ deg

Case	Grid	Δt^*	T^*_{int}	C_l	C_d
Two-dimensional DES	300×75	1×10^{-4}	15	0.148	0.105
Two-dimensional DES	400×100	1×10^{-4}	24	0.308	0.133
Two-dimensional DES	500×125	1×10^{-4}	20	0.309	0.129
Experiment	——	——	——	0.330	——
RANS	400×100	——	——	0.453	0.125

Table 3 Time-step study for iced NACA 23012 at $\alpha = 5$ deg

Case	Grid	Δt^*	T^*_{int}	C_l	C_d
Two-dimensional DES	400×100	1×10^{-4}	15	0.274	0.118
Two-dimensional DES	400×100	5×10^{-4}	40	0.276	0.110
Two-dimensional DES	400×100	1×10^{-3}	70	0.277	0.111
Two-dimensional DES	400×100	2×10^{-3}	120	0.300	0.106
Experiment	——	——	——	0.301	——
RANS	400×100	——	——	0.379	0.096

Compared to RANS predictions, the average C_l predictions from two-dimensional DES with the two different fine grids were closer to the experimental result. Drag coefficients predicted with two-dimensional DES were somewhat higher than for RANS, which was consistent with what was found for the two-dimensional DES validation cases for the cylinder flow. The drag coefficient sensitivity to grid resolution between the two finer grid results indicates that different types of flow patterns may develop with different grid resolutions. However, practical CPU limitations for three-dimensional DES discouraged the use of even high grid resolution. Thus, the 400×100 RANS-type grid was applied in the following three-dimensional DES simulations.

Time-dependent characteristics were also studied for the iced NACA 23012 under the same conditions as earlier with the 400×100 grid at a 5-deg angle of attack. Four different nondimensional time steps ($\Delta t^* = \Delta t U_\infty / c$) of 1×10^{-4}, 5×10^{-4}, 1×10^{-3}, and 2×10^{-3} were used in the simulations. Note that time steps of 1×10^{-2} and 5×10^{-3} (which were used in the cylinder simulations when nondimensionalized with diameter) were also tested but were found to be numerically unstable. This was because the ice-shape size (not the chord length) controls the flow separation, and it was much smaller than the chord length ($k/c = 1.39\%$). As such, the time steps applied here were all from about one to two orders less than those used in cylinder case, which was consistent with the cylinder's flow separation scaling with the entire diameter, whereas it was an order of magnitude less than the airfoil chord.

As shown in Table 3, when the time step increased from 1×10^{-4} to 1×10^{-3}, the effects of different time steps were modest for both the lift and drag predictions. However, when the time step was increased from 1×10^{-3} to 2×10^{-3}, the change in lift predictions was significant. Thus, $\Delta t^* = 1 \times 10^{-3}$ was seen as a reasonable maximum and, thus, was chosen as the baseline time step within this study for the three-dimensional simulations. Compared to lift, drag predictions were less sensitive to the time-step variations, and all of the two-dimensional DES predictions of drag were higher than the RANS predictions as shown before.

DES Spanwise-Domain Grid Consideration

As noted for the cylinder case, DES is a three-dimensional computational methodology. The separated flowfield's three dimensionality should be well represented within the whole DES domain. Thus, the minimum Z-domain size in the simulation should be related to the physical separation bubble size to capture the separation characteristics. However, for the iced airfoil, the separation bubble size varies strongly with angle of attack. To solve this problem, we assumed a linear relationship between the maximum separation

Table 4 Spanwise domain size vs separation bubble height in previous studies

Researchers	Case	Z_{dom}/c	Z_{dom}/H_{sepr}	N_z	A, deg
Travin et al.[7]	DES	2	~2	42	0 (cylinder)
Squires et al.[9]	DES	3	~2–4	151	10 (~cylinder)
Schmidt et al.[18]	LES	0.05	~1	42	12
Dahlstrom and Davidson[19]	LES	0.05	~0.7	33	13.3
Cokljat and Liu[20]	DES	0.03	~1	16	13.3
Shur et al.[6]	DES	1	~1	26	45
Present	DES	Varies	~2	31	Varies

height H_{sepr} for a given separation bubble and spanwise-domain size Z_{dom}. That is,

$$Z_{dom}/H_{sepr} = \text{const}$$

This ratio should be large enough to allow three-dimensional structures to be representative of overall vortex dynamics, but it should also be as small as possible due to computer CPU constraints if a specific Δz resolution were needed. Table 4 shows a range of nondimensional spanwise-domain sizes applied in the previous clean airfoil and cylinder studies and shows the typical number of spanwise grid planes, where $N_z = Z_{dom}/\Delta z$. There was a variety of spanwise domains and resolutions in these studies, but typical values were Z_{dom}/H_{sepr} of about 2 and N_z of about 30.

A total of 31 grid points was specified along the spanwise direction for resolving the flow quantities in present study, consistent with previous studies listed in Table 4. In this study, we also chose the Z_{dom}/H_{sepr} ratio to be 2.0 because iced airfoil separation is more like cylinder flow separation than clean airfoil separation. The Δz based on this selection was about the same order as Δx and Δy in the separated flow regions.

Note that if $H_{sepr} = 0$ (attached flow), then the Z-domain size is also 0, which leads to RANS as the appropriate technique. Also, if H_{sepr} is very small compared to the object, we may not be able to afford to use DES with high resolution within the separation region while still resolving all features of the flow around the object; thus, again, the suggested approach is to use RANS. As such, a flowfield with a significant separation bubble size compared to the body is generally desired if one would employ DES. In this study, a criterion of $H_{sepr}/c > 5\%$ for iced airfoils was used for applying the DES computation. Because H_{sepr} was not measured in the experiments or known a priori, RANS predictions of the separation height $H_{sepr,RANS}$ were applied for each angle of attack. Therefore, all of our angle-of-attack simulations used the following prescription:

$$Z_{dom}/H_{sepr,RANS} = 2.0$$

Three-Dimensional DES for Iced Airfoils

To examine the capability and accuracy of the DES methodology on iced airfoil simulations, the full-domain three-dimensional DES simulations were performed at a series of angles of attack for both the iced NACA 23012 airfoil and the iced NLF 0414 airfoil. The results were compared to the experiments and RANS predictions.

Based on the two-dimensional DES grid and time-step studies, the applied grid had a resolution of $400 \times 100 \times 31$, and the time step was $\Delta t^* = 1 \times 10^{-3}$. Periodic boundary conditions were applied along the spanwise direction. The Courant–Friedrichs–Lewy number was about 0.1 in the LES region with the selected grid configuration and time step. Computations were performed on an IBM AIX system at the National Center for Supercomputing Applications. Grids were divided into eight zones and run in parallel. It took about 9 s of CPU time per cycle, and about 70–100 nondimensional time units were calculated to get averagely converged statistical results.

Three-Dimensional DES for Iced NACA 23012 Airfoil

Full-domain three-dimensional DES simulations were performed at a series of angles of attack for the iced NACA 23012 airfoil at $Re = 2.0 \times 10^6$ and $M = 0.21$. As discussed earlier, the spanwise-domain size was set as twice the maximum separation bubble height

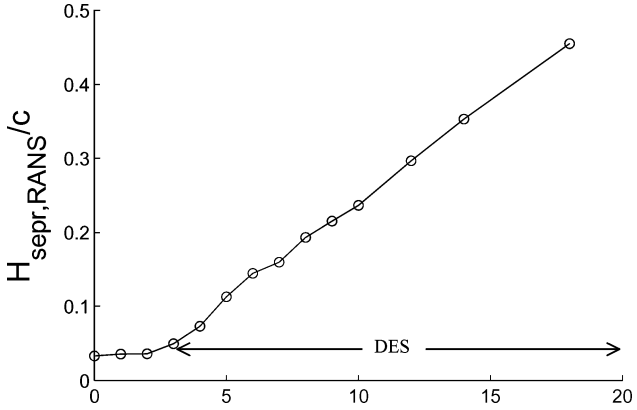

Fig. 6 RANS-predicted separation bubble height of iced NACA 23012 airfoil.

as predicted in RANS ($H_{sepr,RANS}$) at the same angle of attack. The grid spacing increased with angle of attack due to larger separation bubble sizes. Figure 6 shows the separation bubble height at different angles of attack for the iced NACA 23012. The spanwise grid spacing was on the order of 1% of the chord length. This balanced out the grid spacing along the other two directions because Δx and Δy were also about 1% of the chord length in the separated flow region above the airfoil. According to our criterion of $H_{sepr}/c > 5\%$, DES computations should be performed for angles of attack no less than 3 deg. Note that for angles below 3 deg, the flow separation region was small and previous RANS studies showed reasonable predictions.

An instantaneous three-dimensional vorticity isosurface at $t^* = 50$ at $\alpha = 5$ deg is shown in Fig. 7a. Whereas the flow is predominantly two dimensional on the lower surface and along the upper surface in the region of the ice shape, three-dimensional flow structures dominate the flow downstream of the separation region. Figures 7b–7d show the spanwise vorticity contours at the same time as earlier. With strong vortex shedding after the ice-shape location, the variation at the spanwise locations also indicates a well-developed three-dimensional flow structure. An equivalent two-dimensional DES vorticity contour at the same angle of attack is shown in Fig. 7e for comparison. In general, the three-dimensional DES case predicted a much finer and more irregular vortex structure that was not captured in the two-dimensional DES case. (The same trend was found for the cylinder flow.) Figure 8 shows the time evolution of midspan vorticity for the iced NACA 23012 at $\alpha = 5$ deg. The vorticity shedding from the ice shape diffuses and forms more chaotic vortex structures when moving downstream. The strength and position of the shedding vortices changed at different time frames, which led to the variation of lift and drag in their history profiles.

Figure 9a shows the lift history profile at angles of attacks of 5 deg. Unlike the cylinder case, there was no clear primary frequency found from the instantaneous lift coefficients. Note that the lift fluctuations were substantial, which was qualitatively consistent with experiments by Gurbacki for iced airfoils.[21] The time-averaged lift results are also shown where the statistical values were integrated after the initial transient of 20 normalized time units. In general, the average lift and drag converged statistically in about 60 nondimensional time units. Figure 9b shows the averaged pressure distributions compared to the experimental and RANS results. On the upper surface before the ice shape and on the lower surface, there was no significant difference in pressure between the three-dimensional DES and RANS predictions. Both the three-dimensional DES and RANS simulations predict a higher pressure on the lower surface compared to experimental values. The pressure plateaus after the ice shape were predicted much better with three-dimensional DES (as compared to RANS), although the pressure levels above the airfoil were lower compared to the experiments. This indicated that the three-dimensional vortex flow patterns were reasonably captured with three-dimensional DES. Two additional simulations at this angle of attack were run to check influences of ΔZ and Z-domain size.

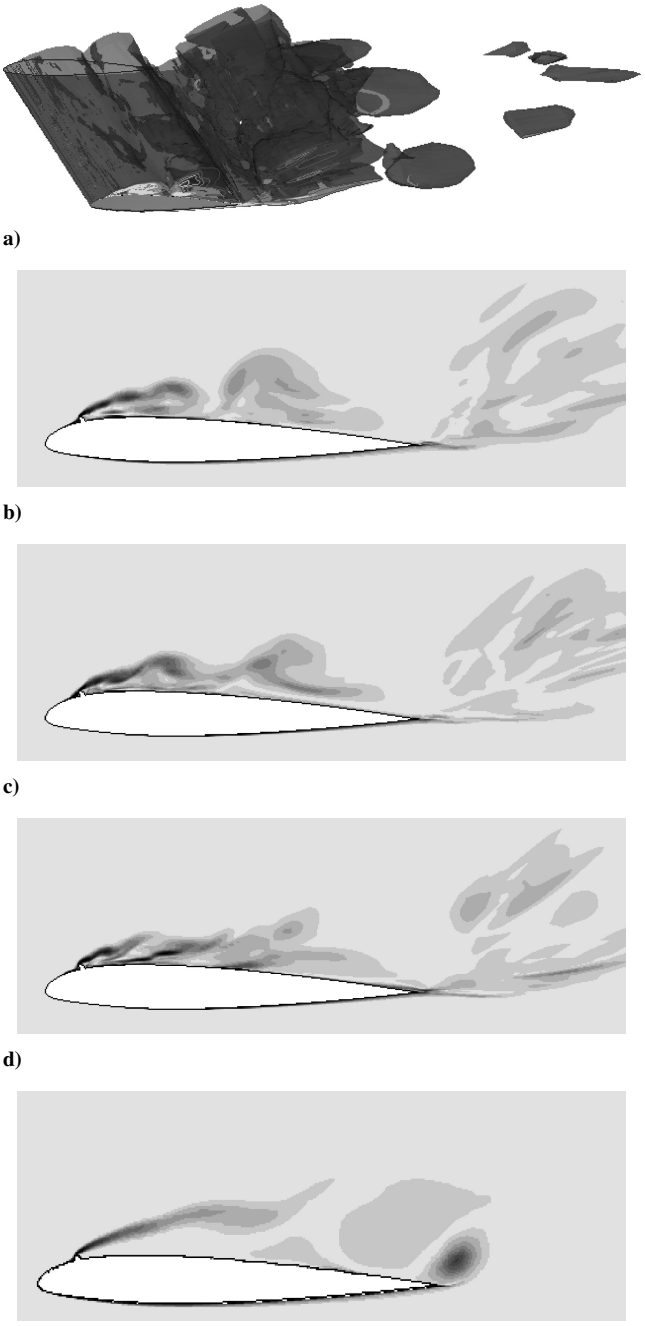

Fig. 7 Instantaneous vorticity contours for iced NACA 23012 at $t^* = 50$ and $\alpha = 5$ deg: a) vorticity isosurface, b) three-dimensional DES at $z = \frac{1}{6} Z_{\text{dom}}$, c) three-dimensional DES at $z = \frac{1}{2} Z_{\text{dom}}$, d) three-dimensional DES at $z = \frac{5}{6} Z_{\text{dom}}$, and e) two-dimensional DES.

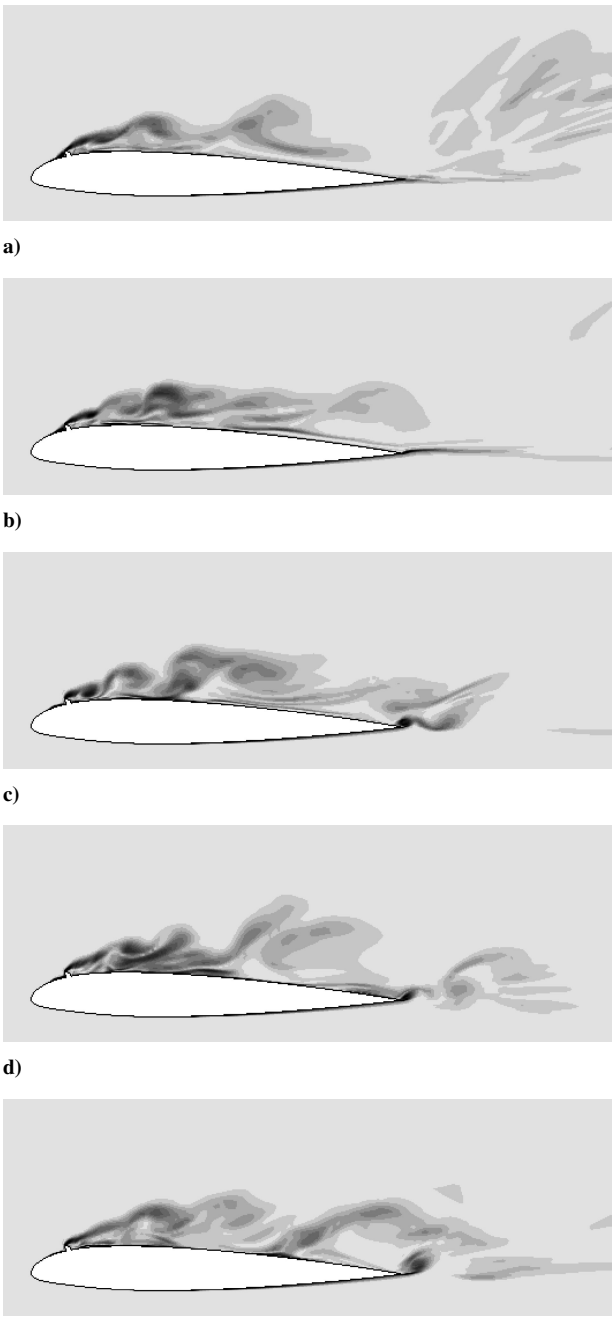

Fig. 8 Midspan spanwise vorticity at different times for iced NACA 23012 with three-dimensional DES at $\alpha = 5$ deg: a) $t^* = 50$, b) $t^* = 50.5$, c) $t^* = 51.0$, d) $t^* = 51.5$, and e) $t^* = 52.0$.

The results were not conclusive, but indicated significant potential for ΔZ influence and possible for Z-domain size influence. Further studies on these two effects are much needed. More DES results on this iced airfoil can be found in Ref. 13.

Figure 10 shows the lift comparisons between RANS and DES predictions. A set number of simulations at $\alpha = 3$, 4, 5, 6, 7, 10, and 14 deg were performed. The calculated values were compared with the Broeren et al. LTPT experimental results.[17] Whereas the predicted lift was generally larger than experimental values around the experimental stall, the DES predictions showed an obvious stall behavior that was not explicitly captured by RANS. Compared to the experimental stall angle of 4 deg, the present three-dimensional DES simulations predicted a 5-deg stall followed by a more severe drop in lift.

Three-Dimensional DES for Iced NLF 0414 Airfoil

DES simulations were also performed for an iced NLF 0414 airfoil for a range of angles of attack around stall. The iced NLF 0414 airfoil has an ice shape of $k/c = 6.67\%$ at a leading-edge location of $s/c = 3.4\%$. The simulations were performed under the condition of a Mach number of 0.185 and a Reynolds number of 1.8×10^6. The numerical predictions were compared to the UIUC experimental results.[22]

Because of the large ice shape applied in this study ($k/c = 6.67\%$), the typical separation bubble usually had a height greater than 5% of chord length than was applicable for the DES simulations. As in the earlier study, only a few angles of attack were considered due to the large computational resources involved. For the NLF 0414 airfoil, four angles of attack of 0, 1, 3, and 5 deg were simulated with the $400 \times 100 \times 31$ grid resolution. These angles were selected because they were close to the experimental stall angle of attack of 1 deg.

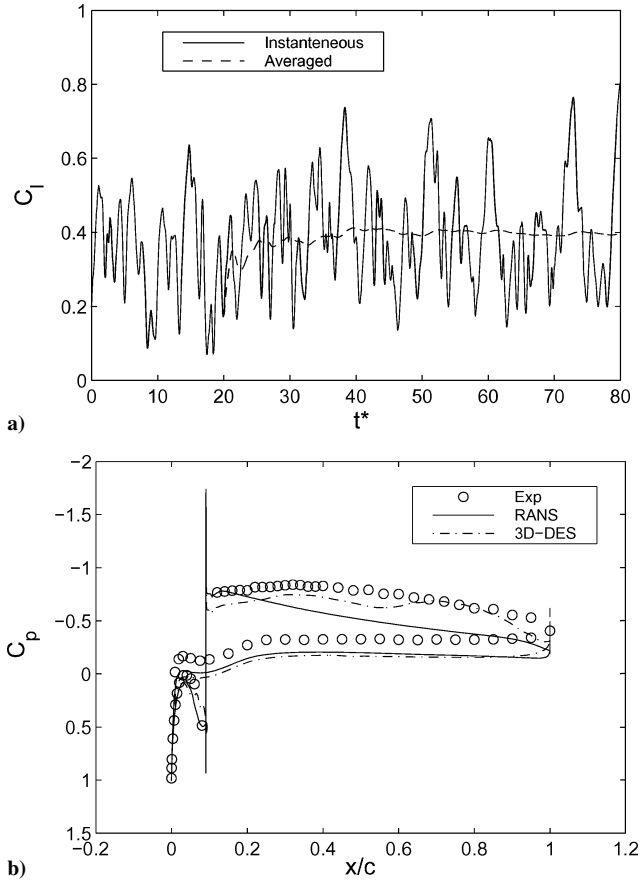

Fig. 9 Time-dependent behavior for iced NACA 23012 at $\alpha = 5$ deg for a) three-dimensional DES instantaneous and time-averaged lift and b) three-dimensional DES time-averaged pressure distribution with comparison to experimental and RANS results.

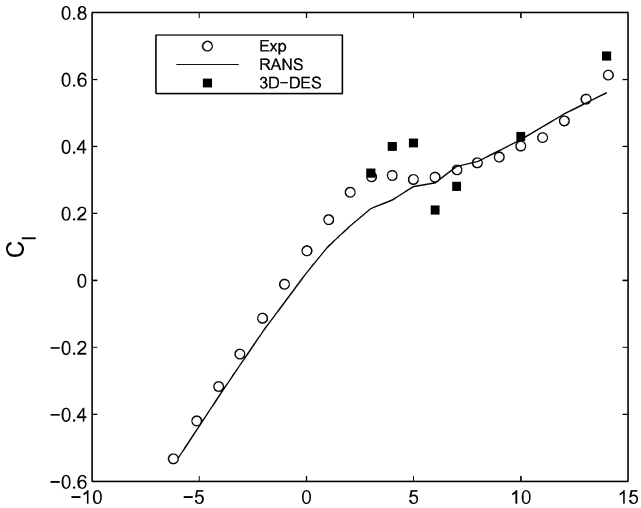

Fig. 10 Three-dimensional DES time-averaged lift coefficient for iced NACA 23012 with comparison to experimental and RANS results.

Figure 11 shows the vorticity isosurface and contours at an instantaneous time frame of $t^* = 50$ at $\alpha = 3$ deg. Compared with the NACA 23012 airfoil with a smaller ice shape of $k/c = 1.39\%$ at $\alpha = 5$ deg, the vorticity isosurface shown in Fig. 11a is distributed over a larger area because of the larger ice shape. Figures 11b–11d show the vorticity contours at different spanwise locations. Significant variance of the shedding vortex in those planes indicates that the flow three dimensionality was well developed, especially after one-half of the chord length. Perhaps due to a larger distance from the airfoil surface, the shear layer formed after the ice shape was

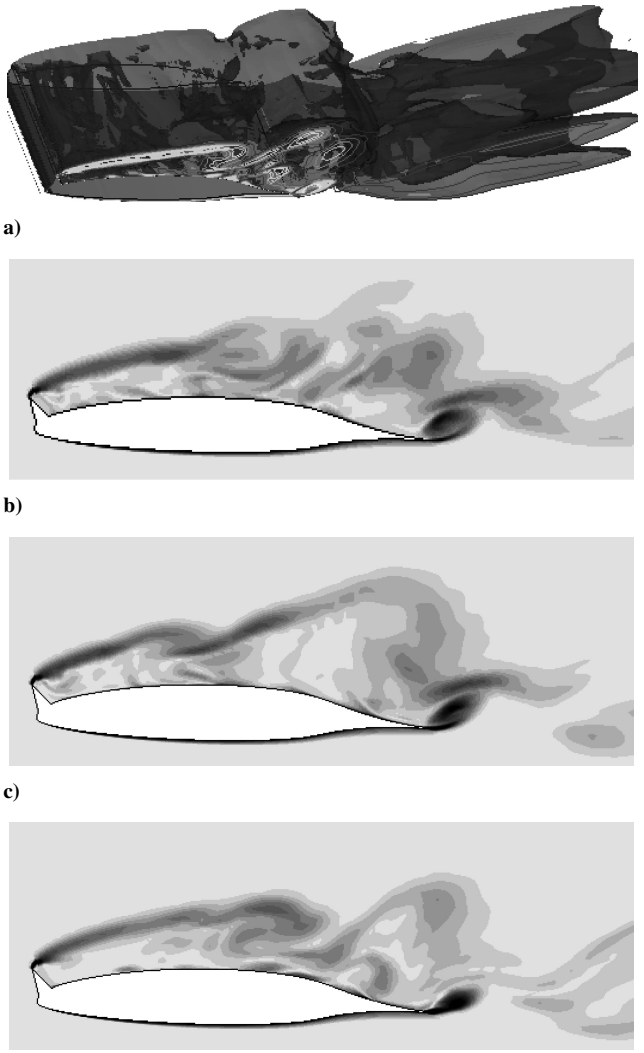

Fig. 11 Instantaneous vorticity contours for iced NLF 0414 flow at $t^* = 50$ and $\alpha = 3$ deg: a) vorticity isosurface, b) three-dimensional DES at $z = \frac{1}{6}\ Z_{\text{dom}}$, c) three-dimensional DES at $z = \frac{1}{2}\ Z_{\text{dom}}$, and d) three-dimensional DES at $z = \frac{5}{6}\ Z_{\text{dom}}$.

more stable than that with the NACA 23012 airfoil with a smaller ice shape. It was also seen that there was a stronger trailing-edge vortex structure existing in the wake.

Figure 12a shows the time-dependent lift behavior of the iced NLF 0414 airfoil at angles of attack of 3 deg. The averaged lift coefficients were integrated from nondimensional time units from 20 to 65 and are also shown. The averaged pressure comparisons are shown in Fig. 12b. The RANS and DES predictions were similar to each other on the lower airfoil surface (consistent with the flow being attached in that region). However, for the upper surface, the RANS predicted a shorter separation bubble and the DES predicted a longer separation bubble (as compared to the experiments). Further research is needed to understand the issues associated with flow separation, recovery, and reattachment predicted by the DES technique. In particular, the effect of spanwise domain and grid resolution (which were explored herein) should be considered.

Figure 13 shows the lift comparisons among experimental results, RANS, and DES numerical predictions. The stall behavior was predicted by DES at $\alpha = 1$ deg, the same as the experimental stall angle (whereas RANS results did not indicate a stall). However, as found in the NACA 23012 case, the DES predicted lift values were significantly larger than the experimental data and then dropped off more severely. Again, studies with a finer grid resolution and increased spanwise domain might be needed to resolve this problem.

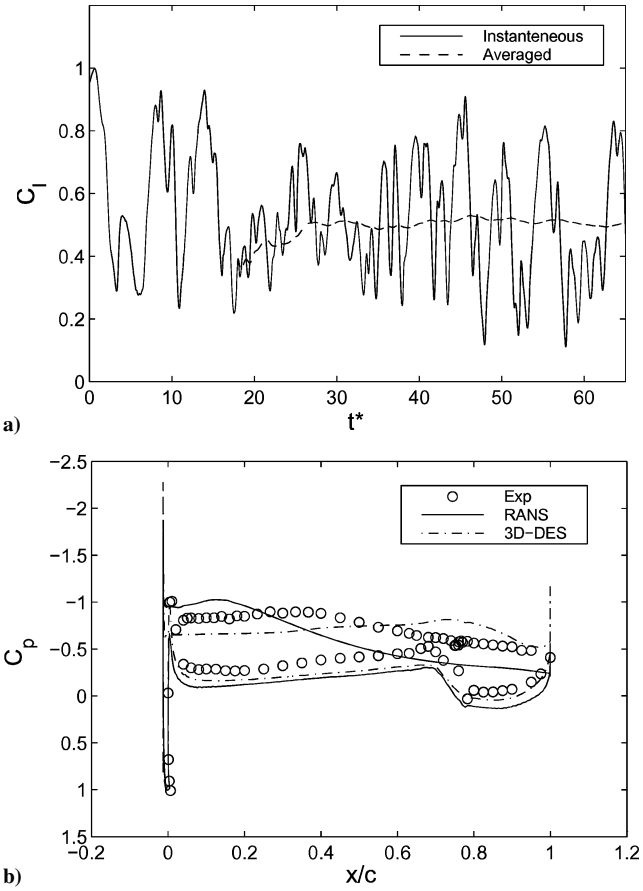

Fig. 12 Time-dependent behavior for iced NLF 0414 at $\alpha = 3$ deg for a) three-dimensional DES instantaneous and time-averaged lift and b) three-dimensional DES time-averaged pressure distribution with comparison to RANS and two-dimensional DES results.

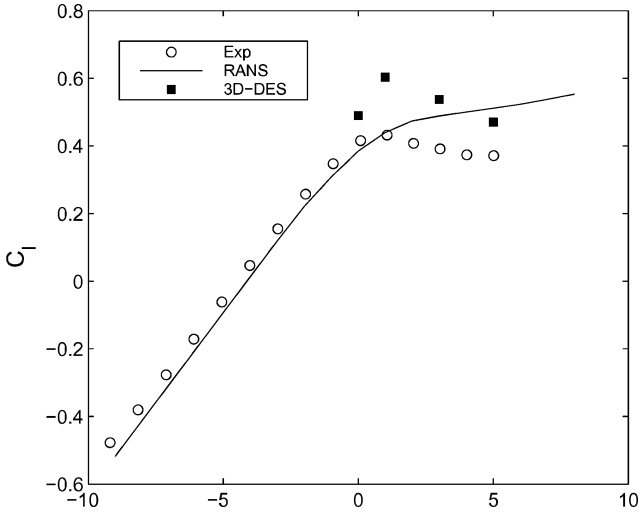

Fig. 13 Three-dimensional DES time-averaged lift coefficient for iced NLF 0414 with comparison to experimental and RANS results.

Summary

The DES methodology was applied in this study to improve flow prediction for the massively separated iced airfoil flow at high angles of attack around stall. The methodology adopted in WIND was first validated with a supercritical separated cylinder flow. The three-dimensional DES results indicated that the flow was substantially three dimensional with much finer vortex structures than those seen in the two-dimensional DES results. The integrated drag and surface pressure for turbulent separated cylinder flow predicted with three-dimensional DES was in good comparison to the experimental result (and better than that of the two-dimensional DES predictions, which were primarily suited for time-step and two-dimensional grid-resolution studies). The frequency of the time-dependent lift history was also reasonably simulated in three-dimensional DES because the Strouhal number was predicted within the experimental range. This confirmed the importance of three dimensionality for DES.

DES simulations were then applied to typical iced NACA 23012 and NLF 0414 airfoils. To form a systematic view of three-dimensional DES on iced airfoils, the simulations were performed for a series of angles of attack for both iced airfoils. Compared to the two-dimensional DES predicted results at the same angles of attack, the vorticity contours shown in the three-dimensional DES provided a much finer flow structure, which is consistent with the cylinder simulations. From the time evolution of vorticity contours at midspan, it is clear that eddies generated at the ice shape diffuse and interact with other eddies when moving downstream. Unlike the cylinder case, there was no obvious frequency for the iced airfoils lift history that is qualitatively consistent with experiments. In addition, the DES predicted lift curve shows an obvious stall behavior consistent with experiments (an aspect that was not predicted with RANS). However, there were significant differences between the DES lift value predictions and the experimental values. Within the comparisons of pressure distributions, the flat plateaus after the ice shape are qualitatively captured in the three-dimensional DES simulation, but at a lower magnitude. On the lower airfoil surface where the flow is attached, the difference between DES and RANS was negligible.

Although DES showed its potential for improving iced airfoil flow simulations, spanwise domain and grid resolution for three-dimensional conditions were not studied in detail due to the large computer resource requirements of DES. A finer grid resolution within the separated flow region is expected to capture the small eddy structures better and the associated flow unsteadiness. Also, adaptive grid techniques and higher-order schemes may improve the fidelity of the resolved eddy aspects of DES.

Acknowledgments

The computations were performed with the support from National Center for Supercomputing Applications and University of Illinois Urbana–Champaign Turing Linux Cluster Systems.

References

[1]Aircraft Owners and Pilots Association Air Safety Foundation, "Aircraft Icing, Safety Advisor: Weather No. 1," B. Landsberg, Frederick, MD, Nov. 2002.

[2]Pan, J., and Loth, E., "Reynolds-Averaged Navier–Stokes Simulations of Airfoils and Wings with Ice Shapes," *Journal of Aircraft*, Vol. 41, No. 4, 2004, pp. 879–891.

[3]Dunn, T., Loth, E., and Bragg, M. B., "Computational Investigation of Simulated Large-Droplet Ice Shapes on Airfoil Aerodynamics," *Journal of Aircraft*, Vol. 36, No. 5, 1999, pp. 836–843.

[4]Kumar, S., and Loth, E., "Aerodynamic Simulations of Airfoils with Upper-Surface Ice Shapes," *Journal of Aircraft*, Vol. 38, No. 2, 2001, pp. 285–295.

[5]Spalart, P. R., Jou, W.-H., Strelets, M., and Allmaras, S. R., "Comments on the Feasibility of LES for Wings, and on a Hybrid RANS/LES Approach," *Advances in DNS/LES*, U.S. Air Force Office of Scientific Research, Greyden Press, Columbus, OH, Aug. 1997.

[6]Shur, M., Spalart, P. R., Strelets, M., and Travin, A., "Detached-Eddy Simulation of an Airfoil at High Angle of Attack," *4th International Symposium on Engineering Turbulence Modeling and Experiments*, Elsevier, Oxford, U.K., 1999, pp. 669–678.

[7]Travin, A., Shur, M., Strelets, M., and Spalart, P. R., "Detached-Eddy Simulations past a Circular Cylinder," *Flow, Turbulence and Combustion*, Vol. 63, Nos. 1–4, 1999, pp. 293–313.

[8]Constantinescu, G. S., and Squires, K. D., "LES and DES Investigations of Turbulent Flow over a Sphere at $Re = 10{,}000$," *Flow, Turbulence, and Combustion*, Vol. 70, Nos. 1–4, 2003, pp. 267–298.

[9]Squires, K. D., Forsythe, J. R., and Spalart, P. R., "Detached-Eddy Simulation of the Separated Flow Around a Forebody Cross-Section," *Direct and Large-Eddy Simulation IV*, European Research Community on Flow, Turbulence and Combustion Series, Kluwer Academic, Dordrecht, The Netherlands, Vol. 8, 2001, pp. 481–500.

[10]Kumar, S., and Loth, E., "Detached Eddy Simulations of an Iced Airfoil," AIAA Paper 2001-0678, Jan. 2001.

[11]Bush, R. H., Power, G. D., and Towne, C. E., "WIND: The Production Flow Solver of the NPARC Alliance," AIAA Paper 98-0935, Jan. 1998.

[12]Spalart, P. R., and Allmaras, S. R., "A One-Equation Turbulence Model for Aerodynamic Flows," *La Recherche Aerospatiale*, Vol. 1, 1994, pp. 1–23.

[13]Pan, J., "Numerical Simulations of Airfoils and Wings," Ph.D. Dissertation, Dept. of Aerospace Engineering, Univ. of Illinois at Urbana–Champaign, Urbana, IL, April 2004.

[14]Roshko, A., "Experiments on the Flow Past a Circular Cylinder at Very High Reynolds Number," *Journal of Fluid Mechanics*, Vol. 10, 1961, pp. 345–356.

[15]van Nunen, J. W. G., "Pressure and Forces on a Circular Cylinder in a Cross Flow at High Reynolds Numbers," *Flow Induced Structural Vibrations*, Springer-Verlag, Berlin, 1974, pp. 748–754.

[16]Lasheras, J. C., and Choi, H., "Three-Dimensional Instablility of a Plane Free Shear Layer: An Experimental Study of the Formation and Evolution of Streamwise Vortices," *Journal of Fluid Mechanics*, Vol. 189, 1988, pp. 53–86.

[17]Broeren, A., Lee, S., LaMarre, C., and Bragg, M. B., "Effect of Airfoil Geometry on Performance with Simulated Ice Accretions, Volume 1: Experimental Investigation," Federal Aviation Administration, Rept. DOT/FAA/AR-03/64, Office of Aviation Research, Washington, DC, Aug. 2003.

[18]Schmidt, S., Franke, M., and Thiele, F., "Assessment of SGS Models in LES Applied to a NACA 4412 Airfoil," AIAA Paper 2001-0434, Jan. 2001.

[19]Dahlstrom, S., and Davidson, L., "Large Eddy Simulation Applied to a High-Reynolds Flow Around an Airfoil Close to Stall," AIAA Paper 2003-0776, Jan. 2003.

[20]Cokljat, D., and Liu, F., "DES of Turbulent Flow over an Airfoil at High Incidence," AIAA Paper 2002-0590, Jan. 2002.

[21]Gurbacki, H., "Iced-Induced Unsteady Flowfield Effects on Airfoil Performance," Ph.D. Dissertation, Dept. of Aerospace Engineering, Univ. of Illinois at Urbana–Champaign, Urbana, IL, Dec. 2003.

[22]Kim, H. S., and Bragg, M. B., "Effect of Leading-Edge Ice Accretion Geometry on Airfoil Aerodynamics," AIAA Paper 99-3150, Jan. 1999.